SEBHA UNIVERSITY CONFERENCE PROCEEDINGS, VOL.03 NO. 2 2024
DOI: 10.51984/SUCP.V3I2.3372

وقائع مؤتمرات جامعة سبها
Sebha University Conference Proceedings

Confrence Proceeeding homepage: http://www.sebhau.edu.ly/journal/CAS

Numerical Implementation of Gradient Enhanced Damage Model for Quasi-Brittle Materials.

*Ibrahim Omar Altarhouni

Department of Civil and Environmental Engineering, Faculty of Engineering, Sebha University, Libya.

Keywords:
Continuum damage mechanics
Gradient enhanced damage
Brittle fracture
Staggered scheme
FEM

A B S T R A C T

Different numerical models have been discussed in recent years to analyze the damage evolution in concrete structures. In this paper, a gradient-enhanced damage model formulation, which is applied to single edge-notched and L-shaped specimens, is explained. A new formulation of the finite element equations is derived, with attention to C^0-continuity requirements. This paper focuses on the derivation of the governing equations as well as the implementation of the model with different mesh discretization and discuss the results of the two examples. The difference between non-local damage mechanics and gradient enhanced damage model is also discussed. The exponential softening evolution law is used to define the damage variable and Mazars model of local equivalent strain is applied to simulate the behavior of the problems.

التنفيذ الرقمي لنموذج الضرر المعزز بالتدرج للمواد شبه الهشة.

*إبراهيم عمر الترهوني

قسم الهندسة المدنية والبيئية، كلية الهندسة، جامعة سبها، ليبيا

الكلمات المفتاحية:
طريقة العناصر المنتهية
المواد الهشة
نموذج الضرر المتدرج
ميكانيكا الضرر

الملخص

تمت في السنوات الماضية مناقشة تطبيق العديد من النماذج الرياضية لتحليل الخواص الفيزيائية والميكانيكية للمواد بمختلف تصنيفاتها، وبالأخص دراسة تطور مراحل انتشار الانهيار في المنشآت الخرسانية والتنبؤ باتجاهات ومسارات هذه التشققات داخل مكونات الخرسانة. في هذه الورقة، تم تقديم التكوين الرياضي لنموذج ضرر تدريجي وتطبيقه على عينة على شكل حرف L وأخرى محتوية على حافة بها حز على شكل V. تم تطوير تكوين جديد لمعادلات العناصر المحددة بمراعاة متطلبات اتصال C_0. تم التركيز في هذه الورقة على استنباط المعادلات الحاكمة وعلى تطبيق النموذج باستخدام تقسيمات (شبكات) مختلفة ومناقشة النتائج المتحصل عليها من النموذجين المختلفين. تم كذلك مناقشة الفرق بين ميكانيكية الضرر غير المحلي والضرر التدريجي. تم استخدام القانون الأسي للانتشار وذلك لتعريف متغيرات الضرر وتم تطبيق نموذج (Mazars) للانفعالات المكافئة المحلية وذلك لمحاكاة سلوك هذه المواد.

1. Introduction

There are many contributions to improve models to describe continuum damage. Damage mechanics theories can be used to describe the failure of structural materials and components by accounting for the degradation of elastic properties due to accumulated damage. For quasi-brittle materials like concrete, these micro-damage processes represent the formation of micro-cracks that occur as the structure is subjected to loading. Regularization techniques are employed in continuum damage models to capture the nonlocal behavior of micro-cracks, which ensures that the governing equations are well-posed. In mechanics, this nonlocal behavior means that the level of damage at a specific point is influenced by the damage in the surrounding area. Alternatively to non-local softening models, there is another interest model called gradient enhanced damage model which presents more advantages over nonlocal models, since they are strictly local in a mathematical sense. The constitutive equations in gradient models are enhanced with additional spatial gradients of state variables [19].

This paper is organized as follows: A basic description of elasticity based on continuum damage model. A gradient formulation of a damage model is derived from the non-local theory. The report covers the numerical solutions by examining the spatial discretization of the governing equations and presenting a consistent procedure for solving the resulting equations. It describes the foundational models, including the continuum damage models as well as the nonlocal and gradient-enhanced damage models. The report then progresses to derive the finite element formulation and conduct numerical validation. Finally, it concludes with results from numerical simulations used to validate

*Corresponding author:
E-mail addresses: ibr.altarhouni@sebhau.edu.ly

Article History : Received 20 June 2024 - Received in revised form 28 September 2024 - Accepted 06 October 2024

the model.

2. Continuum Damage Theory

The basic concept of continuum damage mechanics is that microstructural defects (micro cracks, micro voids) in a material. As it is illustrated in Figure (1), the microstructural defects can be represented by a set of continuous damage variables. The value of the damage variable ω at a specific point in the continuum indicates the quantity and magnitude of defects within a small volume at that location.

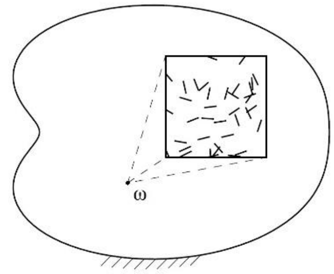

Fig. 1: Damage variable as a representation of microstructural defects [14].

After a certain amount of loading, three regions can generally appeared in the material domain Ω as is shown in Figure (2). In part Ω_0 of the domain, no damage may have developed. The damage variable still has its initial value = zero in this region and the material properties still have the virgin values. In the second region Ω_d, damage has already occurred, but the damage is not yet critical *(0 < ω < 1)*. The limiting value *ω* = 1 has been reached in the third region Ω_c, i.e., in this region the mechanical properties and strength have been completely lost. The completely damaged region Ω_c is the continuum damage representation of a crack [14].

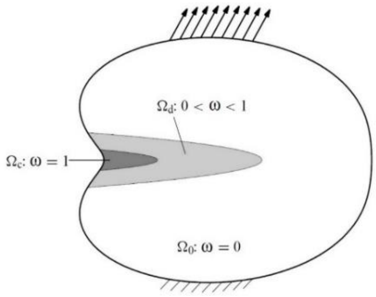

Fig. 2: Damage distribution in a continuum [14].

2.1 Quasi-Brittle Damage:

Quasi-brittle fracture refers to fracture processes where, although there is not significant large-scale plastic deformation, more energy is required to create the crack surface than is typically needed. Figure (3) illustrates the stress-strain response observed in tensile tests of concrete specimens when the load is removed at regular intervals (e.g., Mazars and Pijaudier-Cabot; Shah and Maji, 1989) [14]. In this diagram, the strain represented is an average strain [14]. A softening behavior in the damaged region can be caused by the decrease of stiffness after damage initiation. Softening means that the load-carrying capacity will decrease with increasing deformation and its evolution depends on the material characteristics.

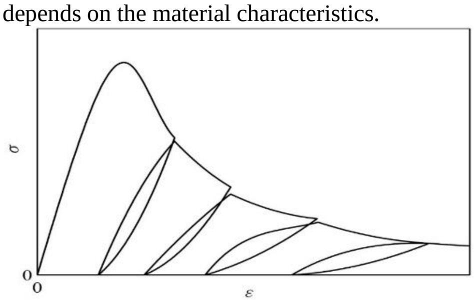

Fig. 3: Stress-strain response of concrete in tension [14].

2.2 Nonlocal Damage Mechanics.

In the standard damage model, damage tends to become localized in an increasingly small volume, often much smaller than the size of the microstructural elements. This localized damage distribution conflicts with the assumed smoothness of the damage variable [14]. Figure (4) illustrates how non-local models smooth deformation and prevent damage from localizing to a single surface. Instead of relying solely on the strain history at a specific point, these models also consider the strain field in the surrounding area.

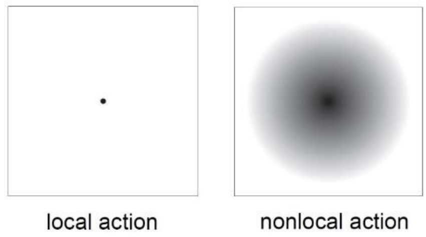

Fig. 4: local and nonlocal action [18].

In nonlocal damage theory, damage is determined not by the local equivalent strain ε_{eq} but by its nonlocal equivalent $\bar{\varepsilon}_{eq}$. Consequently, the loading/unloading function is reformulated by substituting the local equivalent strain with its nonlocal counterpart, which are now expressed as: $f = \bar{\varepsilon}_{eq} - \kappa$ (1)

2.4 Gradient-Enhanced Damage Model

Since the nonlocal model has some disadvantages that the model has convergence problems due to inconsistent tangent operators. In the gradient enhancement model, the nonlocal model is transformed into a gradient-dependent formulation [13]. This is achieved by deriving a gradient formulation directly from the nonlocal theory, which involves expanding the local equivalent strain into a Taylor series as follows:

$$\varepsilon_{eq}(x+\xi) = \varepsilon_{eq}(x) + \nabla\varepsilon_{eq}(x).\xi + \frac{1}{2!}\nabla^2\varepsilon_{eq}(x).\xi^2 + \frac{1}{3!}\nabla^3\varepsilon_{eq}(x).\xi^3 + \frac{1}{4!}\nabla^4\varepsilon_{eq}(x).\xi^4 + \cdots \quad (2)$$

where ∇^n represents the nth -order gradient operator and ξ^n denotes the nth -order dyadic product of *ξ*, respectively. Applying some basic algebraic operations, a gradient formulation can be expressed as

$$\bar{\varepsilon}_{eq} = \varepsilon_{eq} + c\,\nabla^2\varepsilon_{eq} + d\,\nabla^4\varepsilon_{eq} + \cdots \quad (3)$$

The constants *c* and *d* involve the mathematical operation of integrating the weight function $g(\xi)$ with respect to the positive vector *ξ*. The last step is neglecting the higher order terms from expression (3) and gives the following definition [2]

$$\bar{\varepsilon}_{eq} = \varepsilon_{eq} + c\,\nabla^2\varepsilon_{eq} \quad (4)$$

In this expression, the nonlocal equivalent strain is expressed explicitly in terms of the local equivalent strain, leading to what is known as the explicit gradient-enhanced damage model. This model has a disadvantage that a high order interpolation for the displacement is required. To avoid this point, the implicit gradient enhanced damage model can be used where the nonlocal equivalent strain is written as an implicit form on the local field as $\bar{\varepsilon}_{eq} - c\,\nabla^2\bar{\varepsilon}_{eq} = \varepsilon_{eq}$ (5)
which is the C^0-continuity is required in the formulation. The constant parameter *c* can be defined from the square of the length scale as following $c = 0.5\,.\,l_c^2$ (6)

In order to solve the partial differential equation (5), additional boundary conditions are required regarding the equivalent strain $\bar{\varepsilon}_{eq}$ have to be specified. Mathematically, the non-local equivalent strain $\bar{\varepsilon}_{eq}$ or the normal derivative $\vec{\nabla}\bar{\varepsilon}_{eq}.\vec{n}$ should be defined in every boundary condition. Although no physical foundation exists, the homogeneous Neumann condition has been proved to give reasonable results [15] $\nabla\,.\,\bar{\varepsilon}_{eq} = 0$ on Γ (7)

3. Finite Element Implementation

Since it is difficult to obtain an analytical solution of the governing equations with damage and fracture problems even for simple geometries and loading conditions, the numerical approach is required to solve the Practical problems with complex geometries and non-uniform loading. The equilibrium partial differential equations are discretized in space by a finite element interpolation. An iterative procedure is used to solve the resulting set of nonlinear algebraic equations [14].

3.1 Governing Equations

The governing equations for quasi-static solids with a gradient-enhanced damage model ,summarized as follows, include the equilibrium equations and the implicit relationship between the nonlocal equivalent strain and the local equivalent strain. [12]

- *Equilibrium equation* $\nabla . \sigma + \mathrm{b} = 0$ in Ω (8)
- *Non-local equivalent strain* $\bar{\varepsilon}_{eq} - c\, \nabla^2 \bar{\varepsilon}_{eq} = \varepsilon_{eq}$ in Ω (9)
- *Constitutive equation* $\sigma_{ij} = (1 - \omega)\, C_{ijkl}\, \varepsilon_{kl}$ (10)
- *Damage evolution law* $\omega = f(\kappa)$ (11)
- *Loading function* $f = \bar{\varepsilon}_{eq} - c$ (12)
- *Loading/unloading condition (Kuhn-Tucker condition)*

$$f \le 0 \qquad \dot{\kappa} \ge 0 \qquad f\,\dot{\kappa} = 0 \tag{13}$$

- *Local equivalent strain* $\varepsilon_{eq} = g(\varepsilon)$ (14)
- *Boundary conditions* $\mathrm{u} = \bar{\mathrm{u}}$ on Γ_u (15)

$$\mathrm{n} . \sigma = \bar{\mathrm{t}} \quad \text{on } \Gamma_t \tag{16}$$

$$\nabla . \bar{\varepsilon}_{eq} = 0 \quad \text{on } \Gamma \tag{17}$$

3.2 Discretization

Transforming the governing equations into their weak form is used to reduce the order of the derivatives appearing in these equations. For this step, the Bubnov-Galerkin method is used to discretize the weak form of the governing equations. At the element level, the displacement and the nonlocal equivalent strain fields associated with the weight functions are discretized as follows:

$$u^h = N_u\, \mathrm{u}, \quad w_u^h = N_u\, w_u, \quad \bar{\varepsilon}_{eq} = N_\varepsilon\, \bar{\varepsilon}_{eq}, \quad w^h_{\bar{\varepsilon}_{eq}} = N_{\bar{\varepsilon}_{eq}}\, w_{\bar{\varepsilon}_{eq}},$$
$$\nabla w_u^h = B_u\, w_u, \quad \nabla w^h_{\bar{\varepsilon}_{eq}} = B_{\bar{\varepsilon}_{eq}}\, w_{\bar{\varepsilon}_{eq}}, \qquad \nabla \bar{\varepsilon}^h_{eq} = B_{\bar{\varepsilon}_{eq}}\, \bar{\varepsilon}_{eq} \tag{18}$$

By substituting relations (18) into the weak formulation of the governing equations and expressing the stress and strain tensors in vector form, we obtain:

$$\int_\Omega w_u^T\, B_u^T\, \sigma\, d\Omega = \int_\Omega w_u^T\, N_u^T\, b\, d\Omega + \int_{\Gamma_t} w_u^T\, N_u^T\, \hat{t}\, d\Gamma \tag{19}$$

$$\int_\Omega w^T_{\bar{\varepsilon}_{eq}}\, B_\varepsilon^T\, c\, B_\varepsilon\, \bar{\varepsilon}_{eq}\, d\Omega + \int_\Omega w^T_{\bar{\varepsilon}_{eq}}\, N_\varepsilon^T\, N_\varepsilon\, \bar{\varepsilon}_{eq}\, d\Omega = \int_\Omega w^T_{\bar{\varepsilon}_{eq}}\, N_\varepsilon^T\, \varepsilon_{eq}\, d\Omega \tag{20}$$

which must be valid for any choice of w_u and $w_{\bar{\varepsilon}_{eq}}$. Consequently, the final discretized form of the governing equations is: [17]

$$\int_\Omega B_u^T\, \sigma\, d\Omega = \int_\Omega N_u^T\, b\, d\Omega + \int_{\Gamma_t} N_u^T\, \hat{t}\, d\Gamma \tag{21}$$

$$\int_\Omega B_\varepsilon^T\, c\, B_\varepsilon\, \bar{\varepsilon}_{eq}\, d\Omega + \int_\Omega N_\varepsilon^T\, N_\varepsilon\, \bar{\varepsilon}_{eq}\, d\Omega = \int_\Omega N_\varepsilon^T\, \varepsilon_{eq}\, d\Omega \tag{22}$$

3.2 Linearization

Equations (21, 22) are the coupled equations to be solved. Since they are nonlinear equations, they must be linearized. According to the Newton-Raphson method, the linearized change $\delta\sigma_i$ of the stress column σ in iteration i, is obtained starting from the matrix representation [15] $\sigma = (1 - \omega)\, C\, \varepsilon$ (23)
of the stress-strain relation. Differentiating equation (23) , we get:

$$\dot{\sigma} = (1 - \omega)\, \mathbb{C}^{el}\, \dot{\varepsilon} - \mathbb{C}^{el}\, \varepsilon\, \dot{\omega} \tag{24}$$

For the first term on the right-hand side, applying $\varepsilon = b(u) = \underline{B}\, u$ directly gives: [15] $\delta\varepsilon_i = \underline{B}\, \delta u_i$ (25)

where
$$B_\varepsilon = \begin{bmatrix} \frac{\partial}{\partial x} \\ \frac{\partial}{\partial y} \\ \frac{\partial}{\partial z} \end{bmatrix} [N_1 \ \ N_2 \ \ \dots\dots\dots \ \ N_n] \tag{26}$$

and
$$\begin{aligned} \dot{\omega} &= \frac{\partial\omega}{\partial\kappa}\, \dot{\kappa} \\ &= \frac{\partial\omega}{\partial\kappa}\, \frac{\partial\kappa}{\partial\varepsilon_{eq}}\, \dot{\varepsilon}_{eq} \\ &= \frac{\partial\omega}{\partial\kappa}\, \frac{\partial\kappa}{\partial\varepsilon_{eq}}\, \frac{\partial\varepsilon_{eq}}{\partial\varepsilon}\, \dot{\varepsilon} \end{aligned} \tag{27}$$

The Kuhn-Tucker relations (13) indicate that if damage increases (κ >0), the history parameter satisfies κ = ε_{eq}, so $\delta\kappa = \delta\varepsilon_{eq}$. If no damage increase occurs, $\boldsymbol{i}$ is given by $= 0$. When damage does occur, $\boldsymbol{i}$ is determined by comparing the current value of the non-local equivalent strain to the converged value κ_i of the history parameter from the previous increment. Thus, the change in damage $\delta\omega_i$ can be linearized as:

$$\delta\omega_i = \frac{\partial\omega}{\partial\kappa}\, \dot{\bar{\varepsilon}}_{eq} = \frac{\partial\omega}{\partial\kappa}\, N\, \dot{\bar{\varepsilon}}_{eq} \tag{28}$$

The parameter $\frac{\partial\kappa}{\partial\varepsilon_{eq}}$ in eqn. (27) is equal to 1 for loading and 0 otherwise.

Combining (25) and (28) yields

$$\dot{\sigma} = (1 - \omega)\, \mathbb{C}^{el}\, B_u\, \dot{\mathrm{u}} - \frac{\partial\omega}{\partial\kappa}\, \frac{\partial\kappa}{\partial\varepsilon_{eq}}\, \mathbb{C}^{el}\, \varepsilon\, N_\varepsilon\, \dot{\bar{\varepsilon}}_{eq} \tag{29}$$

Thus, the iterative change in the internal nodal forces can be expressed as:
$$\delta f^u_{int} = \int_\Omega B_u^T \sigma B\, d\Omega\, \delta u - \int_\Omega B_u^T \left(\mathbb{C}^{el}\, \varepsilon\, \frac{\partial\omega}{\partial\kappa}\, \frac{\partial\kappa}{\partial\bar{\varepsilon}_{eq}} \right) N_\varepsilon d\Omega\, \delta\bar{\varepsilon}_{eq} \tag{30}$$

Applying this expression to the discrete equilibrium equation for iteration i results in:

$$-K_{uu}\, \delta u - K_{u\varepsilon}\, \delta\bar{\varepsilon}_{eq} = f^u_{int} - f^u_{ext} \tag{31}$$

where the stiffness matrices read

$$K_{uu} = \int_\Omega B_u^T\, \left((1 - \omega)\, \mathbb{C}^{el} \right) B_u\, d\Omega \tag{32}$$

$$K_{u\varepsilon} = -\int_\Omega B_u^T\, \left(\mathbb{C}^{el}\, \varepsilon\, \frac{\partial\omega}{\partial\kappa}\, \frac{\partial\kappa}{\partial\bar{\varepsilon}_{eq}} \right) N_\varepsilon\, d\Omega \tag{33}$$

and the nodal force vectors are given by

$$f^u_{ext} = \int_\Omega N_u^T\, b\, d\Omega + \int_{\Gamma_t} N_u^T\, \hat{t}\, d\Gamma \tag{34}$$

$$f^u_{int} = \int_\Omega B_u^T\, \sigma\, d\Omega \tag{35}$$

In the same manner, the linearization of the relation (22) gives

$$K_{\varepsilon u}\, \delta u - K_{\varepsilon\varepsilon}\, \delta\bar{\varepsilon}_{eq} = -K_{\varepsilon\varepsilon} . \bar{\varepsilon}_{eq} + \int_\Omega N_\varepsilon^T\, \varepsilon_{eq}\, d\Omega \tag{36}$$

where
$$K_{\varepsilon u} = -\int_\Omega N_\varepsilon^T\, \left[\frac{\partial\varepsilon_{eq}}{\partial\varepsilon} \right]^T B_u\, d\Omega \tag{37}$$

$$K_{\varepsilon\varepsilon} = \int_\Omega \left(B_\varepsilon^T\, c\, B_\varepsilon + N_\varepsilon^T\, N_\varepsilon \right) d\Omega \tag{38}$$

The linearized equilibrium and diffusion equations are summarized by combining Equations (31) and (36) in the following system of equations [17]:

$$\begin{bmatrix} K_{uu} & K_{u\varepsilon} \\ K_{\varepsilon u} & K_{\varepsilon\varepsilon} \end{bmatrix} \begin{bmatrix} \delta u \\ \delta\varepsilon \end{bmatrix} = \begin{bmatrix} f_{ext} \\ 0 \end{bmatrix} - \begin{bmatrix} f^u_{int} \\ f^\varepsilon_{int} \end{bmatrix} \tag{39}$$

with the internal nodal force vector

$$f^\varepsilon_{int} = K_{\varepsilon\varepsilon} . \bar{\varepsilon}_{eq} - \int_\Omega N_\varepsilon^T\, \varepsilon_{eq}\, d\Omega \tag{40}$$

3.4 Derivatives of equivalent strain w.r.t strains

The derivatives of the equivalent strain with respect to the strain vector are used to compute the tangent stiffness matrix in damage models, and they are given by:

$$\left[\frac{\partial\varepsilon_{eq}}{\partial\varepsilon} \right]^T = \left\{ \frac{\partial\varepsilon_{eq}}{\partial\varepsilon_1}, \ \frac{\partial\varepsilon_{eq}}{\partial\varepsilon_2}, \ \frac{\partial\varepsilon_{eq}}{\partial\varepsilon_3} \right\} \tag{41}$$

In this paper, the Mazars model will be used to define the equivalent strain criterion to simulate the behavior of specimens.

3.4.1 Mazars equivalent strain

In two dimensions, there are three principal strains. Two of these are solutions to the following quadratic equation:

$$\varepsilon_i^{\,2} - \left(\varepsilon_{xx} + \varepsilon_{yy} \right) \varepsilon_i + \varepsilon_{xx}\varepsilon_{yy} - \varepsilon_{xy}^{\,2} = 0 \tag{42}$$

Namely
$$\varepsilon_{1,2} = \frac{(\varepsilon_{xx} + \varepsilon_{yy}) \pm d}{2} \tag{43}$$

with d given by
$$d = \sqrt{\left(\varepsilon_{xx} + \varepsilon_{yy} \right)^2 + 4\, \varepsilon_{xy}^{\,2}} \tag{44}$$

The last principal strain is
$$\varepsilon_3 = -\frac{\nu}{1 - \nu} \left(\varepsilon_{xx} + \varepsilon_{yy} \right) \tag{45}$$

3.5 Solution algorithm

The algorithm for solving the system of equations with full Newton-Raphson method is summarized in Box (1). Since fully coupled implicit models are more difficult to implement, the staggered approach is used to solve the system of equations.

Box (1): Flowchart for gradient-enhanced damage model with full Newton-Raphson

1. Initialization: $u = 0$, $n = 0$.
2. using the displacement increment, Estimate next solution u_{new}
3. in the increment step level

3.1. Start the iterative process to solve for the displacement:
 3.1.1. Determine the stiffness matrix K_{uu}.
 3.1.2. Determine the force vector f^u_{int}.
 3.1.3. Apply the essential boundary conditions.
 3.1.4. Solve the system of equation for δu.
 3.1.5. Check for convergence, if not go to step 3.1.1.
 3.1.6. update the displacement quantities $u_{n+1} = u_n + \delta u$

3.2. Start the iterative process to solve the non-local equivalent strain:
 3.2.1. Use the updated displacement in the last iterative process u_{n+1}.
 3.2.2. Determine the stiffness matrix $K_{\varepsilon\varepsilon}$.
 3.2.3. Determine the force vector f^ε_{int}.
 3.2.4. Solve the system of equations for $\delta\bar{\varepsilon}_{eq}$.
 3.2.5. Check for convergence, if not go to step 3.2.2.

3.2.6. Update the non-local equivalent strain quantities $\bar{\varepsilon}_{eq,n+1} = \bar{\varepsilon}_{eq} + \delta\bar{\varepsilon}_{eq,n}$.

4. Update displacement u_{n+1} and non-local equivalent strain $\bar{\varepsilon}_{eq,n+1}$.

5. Update the history parameter κ_i where $\kappa_i = \kappa_n$

***At the level of integration points in the iterative process to solve for the displacement:**

1- Compute the local equivalent strain $\varepsilon_{eq,n} = \varepsilon_{eq}(\varepsilon_n)$

2- Evaluate the loading function $f = \bar{\varepsilon}_{eq} - \kappa$

3- Check if loading or unloading $\kappa = \begin{cases} \bar{\varepsilon}_{eq} & , \text{ if } \quad f \geq 0 \\ \kappa_i & , \text{ if } \quad f < 0 \end{cases}$

4- Compute the damage variable $\omega = f(\kappa)$

5- Compute the stress $\sigma = (1 - \omega)\, \mathbb{C}^{el}\ \varepsilon$

4. Numerical Validation

These two examples are solved by the gradient enhanced damage model that is discussed in this paper.

4.1 L-shaped Panel Test

The first example involves testing an L-shaped concrete specimen. The geometry and loading conditions for the L-shaped structure are illustrated in Figure (5). The concrete L-shaped specimen in Figure (5) has been also studied by Zreid, I. (2014) [21].

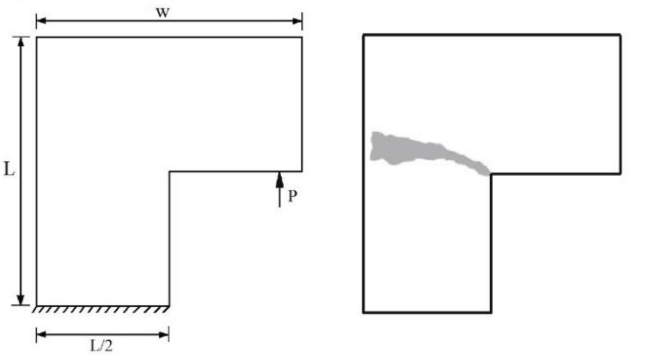

Fig. 5: The geometry and the loading conditions of the L-shaped structure, and experimentally observed crack pattern.

This example is simulated using two different sets of material model and damage parameters for Model 1 and Model 2, as detailed in Table (1) [21]. The local equivalent strain is calculated using the Mazars definition, and the damage evolution follows an exponential softening law. The finite element discretization, consisting of 7500 elements, is depicted in Figure (6).

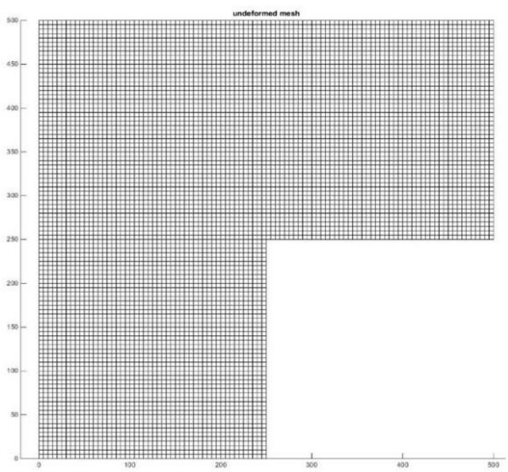

Fig. 6: the element discretization for L-shaped**.**

In this numerical example, the load is applied at the specified position with a displacement increment of 0.04 mm and over 150 steps. The specimen is fixed at the bottom. The nonlinear system has been solved with a full Newton-Raphson method. The convergence criterion is based on the norm of the internal force, with a tolerance of 1.0 × 10^{-8} being selected.

Table 1: Characterization of L-shaped panel test of Model 1 and 2

Geometry and Model Parameters	Quantity		Value: Model 1	Value: Model 2	Unit
Geometry	Width	W	500	500	mm
	Length	L	500	500	mm
Elastic Parameters	Young modulus	E	25.85	18	GPa
	Poisson ratio	ν	0.18	0.18	--
Nonlocal Material Parameter	Gradient parameter	c	1	5	mm²
Damage law	initial damage value	κ_i	0.00125	0.0015	--
	Softening	α	0.96	0.96	--
	Parameters	β	160	450	--

The load-displacement results curves are presented for Model 1 and Model 2 in Figure (7) and Figure (8), respectively.

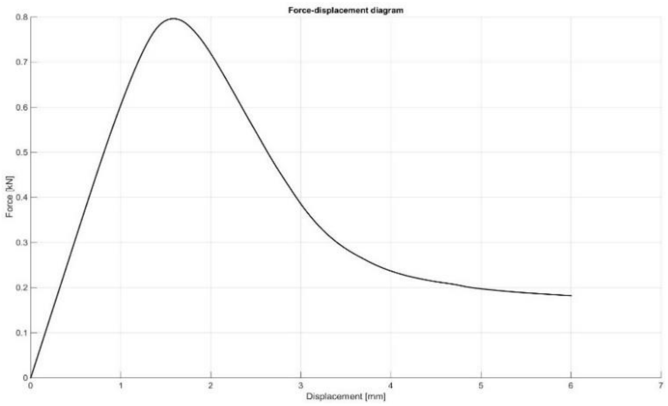

Fig. 7: load-displacement curve for Model 1**.**

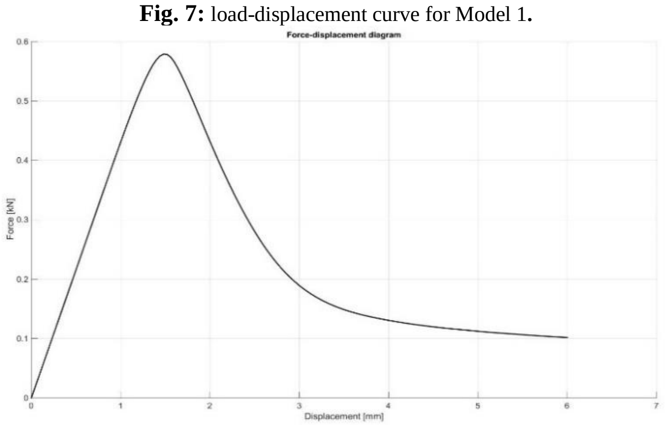

Fig. 8: load-displacement curve for Model 2**.**

The damage patterns at various loading stages for Model 1 are presented, and the displacements at the end of the fracture process, magnified by a factor of 10, are shown in Figure (9).

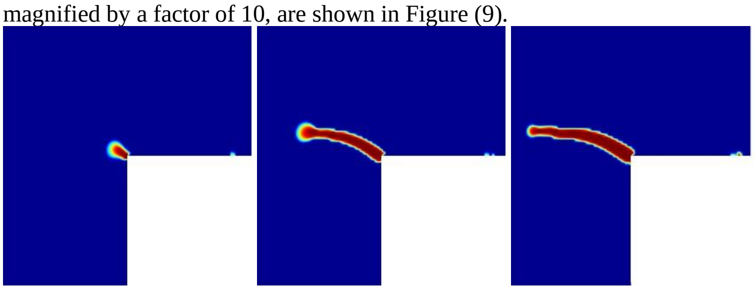

Fig. 9: The damage evolution in the L-shaped structure-Model 1.

where the blue colors indicate undamaged material and the reds refer to fully damaged material. It can be noted that the first damage stage is initiated with less than 90° then continued horizontally to the left edge.

For Model 2, the damage evolution at several stages of loading are presented as well as the deformation at the end of the fracture process is showed with magnified by a factor 10, in Figure (10).

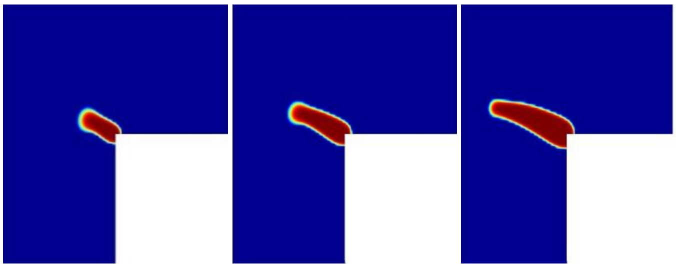

Fig. 10: The damage evolution in the L-shaped structure-Model 2.

It can be observed that in this model, the damage evolution area is larger compared to the previous model, due to differences in the material parameters.

A good convergence has been achieved for implementation of this code. This is illustrated in table (2) below. For example in Model 1, the residual in several steps in case of solving the updated displacement.

Table 2: Convergence at several steps of loading for L-shaped structure

No. of Iterations	Residual		
	Step 80	Step 100	Step 120
Iteration 1	0.13364	0.070672	0.035782
Iteration 2	6.0515 e-13	7.9947 e-13	9.8526 e-13

4.2 Single-edge notched Tension Test

The second example involves testing a single-edge notched mortar specimen. The geometry and loading conditions for the single-edge notched specimen are illustrated in Figure (11). This test has been simulated using two different sets of material model parameters. The first is called (Model 1) and the other is (Model 2). The material model parameters and damage parameters of Model 1 are taken from Nguyen, V. P [12] and are given in the Table (3) while the material model parameters of Model 2 are taken from Benvenuti, E et al [1] and are given in the Table (3) but with different softening parameters.

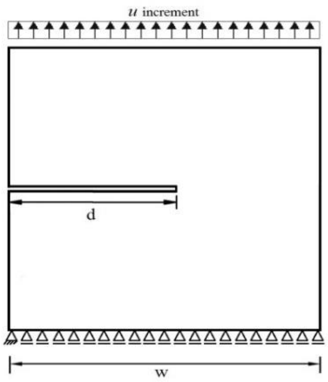

Fig. 11: The geometry and the loading conditions of the Single-edge notched specimen.

The geometry has been analyzed under plane stress conditions. Both models have been analyzed with two different finite element discretization with an increasing fineness of the element mesh in the fracture zone. These discretization meshes consist of 1185 and 3892 elements, respectively.

In this numerical example, a uniform vertical displacement is applied to the top of the specimen. The nodes along the bottom edge are fixed in the y-direction, while the node at the left corner is also fixed in the x-direction. Displacement control is used with increments of Δu = 0.0004 mm and 80 steps for Model 1.

Table 3: Characterization of the single edge notched test of Model 1 and Model 2

Geometry and Model Parameters	Quantity		Value		Unit
			Model 1	Model 2	
Geometry	Width	W	100	100	mm
	Length	L	100	100	mm
	Notch length	d	50	50	Mm
Elastic Parameters	Young modulus	E	35	32.9	GPa
	Poisson ratio	ν	0.2	0.2	--
Nonlocal Material Parameter	Gradient parameter	c	1	1	mm²
Damage law	initial damage value	κ_i	0.05	0.03	--
	Softening	α	0.96	5	--
	Parameters	β	100	0.8	--

For Model 1, the load-displacement results curve is depicted on a medium and a fine mesh in Figure (12) and Figure (13), respectively.

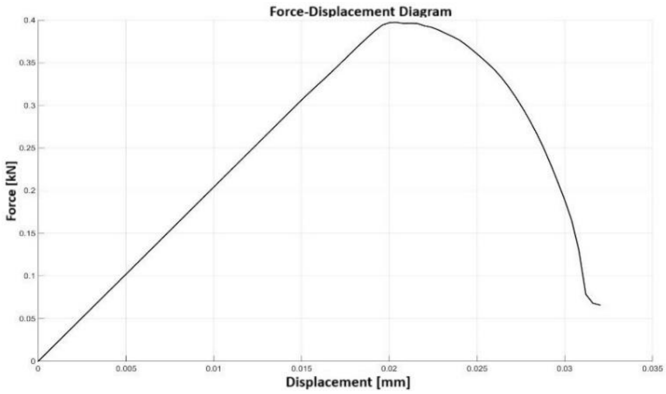

Fig. 12: load-displacement curve for Model 1 – 1185 elements**.**

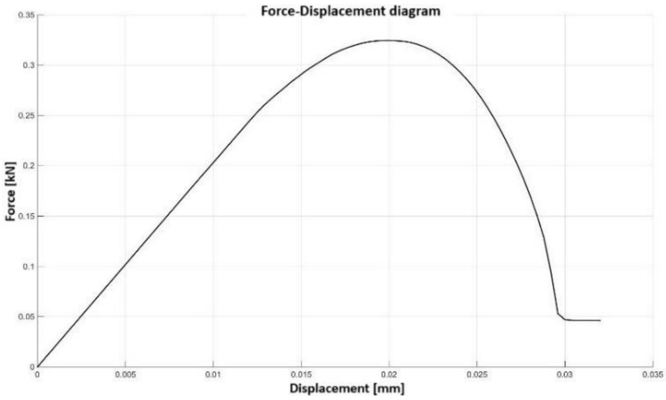

Fig. 13: load-displacement curve for Model 1 – 3982 elements**.**

Good convergence has been achieved for implementation of this code. Table (4) illustrates the convergence at three different steps. For Model 1 in case of solving for the updated displacement.

Table 4: The Convergence at several steps for the single edge notched structure

No. of Iterations	Residual		
	Step 40	Step 50	Step 60
Iteration 1	0.016338	0.022414	0.042863
Iteration 2	4.1067 e-15	5.1836 e-15	6.809 e-15

The nonlinear system has been solved with a full Newton-Raphson method. The convergence criterion is based on the norm of the internal force, with a tolerance of 1.0×10^{-8} being chosen. The local equivalent strain is calculated using the Mazars definition, and the damage evolution follows an exponential softening law.

The damage patterns at several stages loading for Model 1 are presented for medium and fine mesh in Figure (14) and Figure (15), respectively.

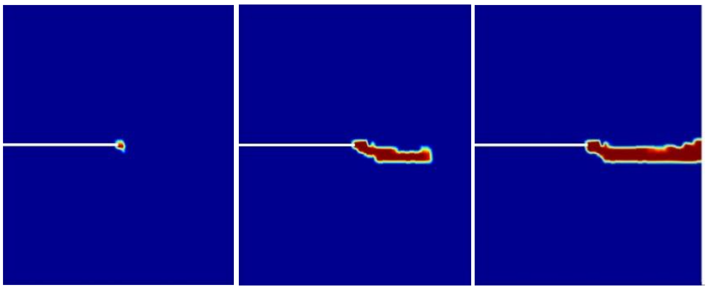

Fig. 14: The damage evolution in the single edge notched with medium Mesh - Model 1**.**

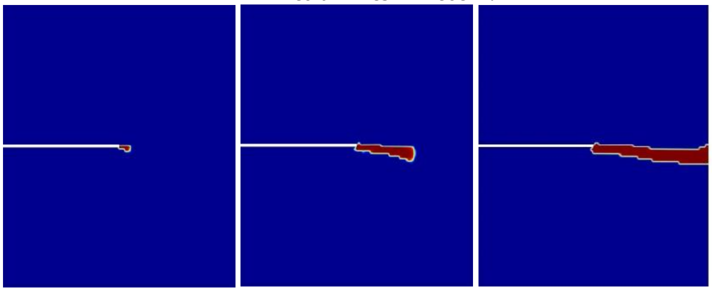

Fig. 15: The damage evolution in the single edge notched with fine Mesh - Model 1**.**

It is evident that, in the initial stage of the fracture process, damage starts at the right side of the notch and progresses to the end of the right edge of the specimen.
For Model 2, the displacement control is used with increments Δu = 0.0005 mm and 80 steps. And the other difference is that the softening parameter, which are used to define the damage variable, are changed. The local equivalent strain is calculated using the Mazars definition, and the damage evolution law follows an exponential softening equation. The load-displacement results curve is depicted on a medium and a fine mesh in Figure (16) and Figure (17), respectively.

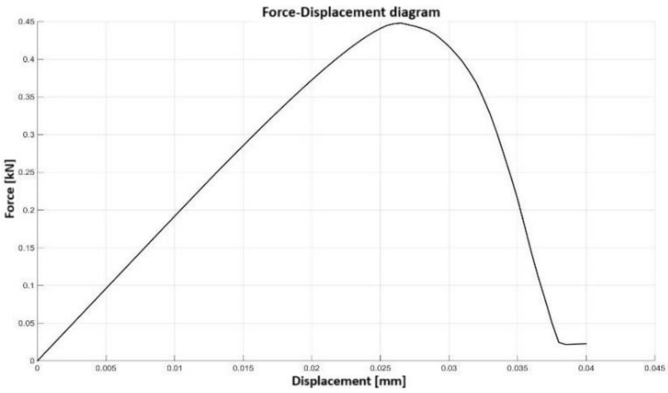

Fig. 16: load-displacement curve for Model 2 – 1185 elements**.**

The damage patterns at several stages loading for Model 2 are presented for medium and fine mesh in Figure (18) and Figure (19), respectively.

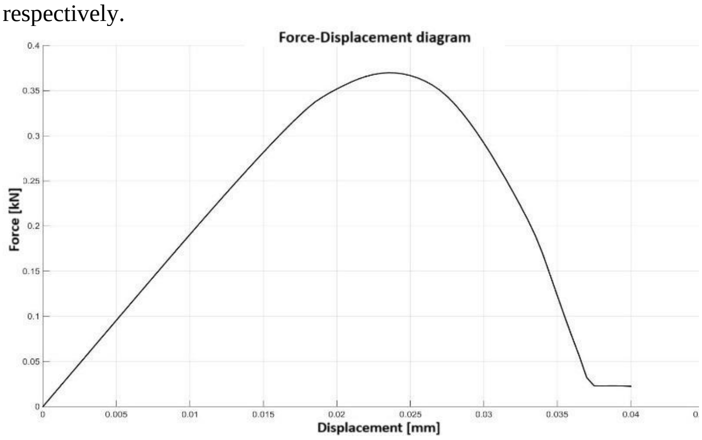

Fig. 17: load-displacement curve for Model 2 – 3982 elements**.**

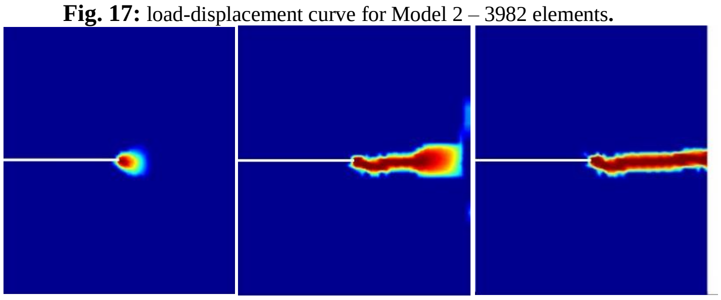

Fig. 18: The damage evolution in the single edge notched with medium Mesh - Model **2.**

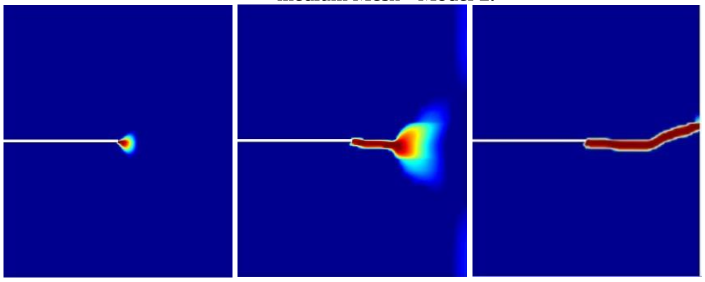

Fig. 19: The damage evolution in the single edge notched with fine Mesh - Model **2.**

5. Conclusion

The implicit gradient-enhanced damage model for quasi-brittle materials, based on non-local theory, has been shown through numerical simulations to accurately represent fracture processes. The explanation covers the implicit gradient enhancement, which improves the strain tensor. It also discusses the linear relationship between the history parameter and the damage variable. Additionally, the integral formulation of the non-local model has been substituted with a partial differential equation that must be solved alongside the equilibrium equation. The independent variables are interpolated separately and both discretization patterns need to satisfy C^0 -continuity. A system of equations is solved using a staggered scheme because fully coupled implicit models are more challenging to implement. This approach is detailed in the algorithm for this model.

6. References

[1]- Benvenuti, E., Loret, B. and Tralli, A., 2004. A unified multifield formulation in nonlocal damage. European Journal of Mechanics A/Solids. S0997-7538(04)00051-8/FLA.
[2]- Bongers, G., 2011. A stress-based gradient-enhanced damage model, A continuum finite element damage model for quasi brittle materials and its finite element method implementation. Master Thesis, Delft University of Technology.
[3]- Bui, Q. V., 2010. Initiation of damage with implicit gradient-enhanced damage models. International Journal of Solids and Structures. 47 (2010) 2425–2435.
[4]- de Borst, R., Pamin, J., Peerlings, R.H.J. and Sluys, L.J., 1995. On gradient-enhanced damage and plasticity models for failure in quasi-brittle and frictional materials. Comp. Mech., 17, 130–141.
[5]- de Borst, R., Benallal, A. and Heeres, O.M., 1996. A gradient-enhanced damage approach to fracture. Pineau, A. and Rousselier, G. (eds.), Proc. 1st European Mechanics of Materials Conf. on Local Approach to Fracture ”86–96”, Journal de Physique IV, vol. 6, 491–502.
[6]- de Borst, R., A class of gradient-dependent damage models for concrete cracking. Fracture Mechanics of Concrete Structures. Proc. FRAMCOS-3, Aedificatio, Freiburg, Germany.
[7]- Desmorat, R., Gatuingt, F. and Ragueneau, F., Nonlocal anisotropic damage model and related computational aspects for quasi-brittle materials. LMT-Cachan, ENS-Cachan/University Paris.
[8]- Geers, M.G.D, de Borst, R. and Peerlings, R.H.J., 1998c. Damage analysis of notched concrete beams loaded in four-point-shear. Mihashi, H. and Rokugo, K. (eds.), Fracture Mechanics of

Concrete Structures. Proc. FRAMCOS-3, Aedificatio, Freiburg, Germany, 981–992.

[9]- Geers, M.G.D, de Borst, R. and Peerlings, R.H.J., 2000. Damage and crack modeling in single-edge and double-edge notched concrete beams. Engineering Fracture Mechanics, 65 (2000) 247-261.

[10]- Giry C, Dufour F, Mazars J (2011) Stress-based nonlocal damage model. International Journal of Solids and Structures, 48(25–26): 3431–3443.

[11]- Mazars, J. and Pijaudier-Cabot, G., 1989. Continuum damage theory - application to concrete. Journal of Engineering Mechanics Division ASCE, 115:345–365.

[12]- Nguyen, V. P., 2008. Continuous and discontinuous modeling of failure in concrete. Computational Mechanics Group. Delft unitversity of Technology. Falculty of Civil Engineering and Geosciences.

[13]- Peerlings, R.H.J., de Borst, R., Brekelmans, W.A.M. and de Vree. J.H.P.,1996. Gradient enhanced damage for quasi-brittle materials. International Journal for Numerical Methods in Engineering, 39:3391–3403, 1996.

[14]- Peerlings, R.H.J., 1999. Enhanced damage modelling for fracture and fatigue. PhD thesis, Eindhoven University of Technology.

[15]- Peerlings, R.H.J., de Borst, R., Brekelmans, W.A.M. and de Vree. J.H.P. computational modeling of gradient-enhanced damage for fracture and fatigue problems. Eindhoven University of Technology, Faculty of Mechanical Engineering.

[16]- Peerlings, R.H.J., de Borst, R., Brekelmans, W.A.M. and Geers, M. G. D., 1998. Gradient-enhanced damage modelling of concrete fracture. Mechanics of Cohesive-Frictional Material. 3, 323-342.

[17]- Saroukhani, S., Vafadari, R. and Simone, A., 2013. A simplified implementation of a gradient-enhanced damage model with transient length scale effects. Comput Mech., 1:899–909.

[18]- Simone, A., 2007. Explicit and implicit gradient-enhanced damage models. ALERT Graduate School, October 13, 2007, Aussois, France.

[19]- Simone, A., Askes, H., Peerlings, R. H. J. and Sluys, L. J., 2003. Interpolation requirements for implicit gradient-enhanced continuum damage models. Communications in Numerical Methods in Engineering, 19:563–572.

[20]- Waffenschmidt, T., Polindara, C. and Menzel, A., 2015. A Gradient-Enhanced Continuum Damage Model for Residually Stressed Fibre-Reinforced Materials at Finite Strains. Lecture Notes in Applied and Computational Mechanics 74, DOI 10.1007/978-3-319-10981-7_2.

[21]- Zreid, I. and Kaliske, M., 2014. Regularization of microplane damage models using an implicit gradient enhancement. International Journal of Solids and Structures DOI: 10.1016/j.ijsolstr.2014.06.020.

[22]- Winkler, B., 2001. Traglastuntersuchungen von unbewehrten und bewehrten Betonstrukturen auf der Grundlage eines objektiven Werkstoffgesetzes fürBeton, Dissertation. University of Innsbruck, Austria.